Electromagnetic radiation at extreme angular velocity

Matteo Buzzegoli and Kirill Tuchin

Department of Physics and Astronomy, Iowa State University,
2323 Osborn Drive, Ames, IA 50011, U.S.A.

E-mail: mbuzz@iastate.edu, tuchink@gmail.com

ABSTRACT: We consider a system rotating at extremely high angular velocity, so that its matter is found mostly at the light-cylinder. We posit that it can be described by quantum fields confined to the two-dimensional cylindrical surface rotating about its symmetry axis. We apply this model to study the electromagnetic radiation. In particular, we compute the photon spectrum emitted by the quark-gluon plasma.

Contents

1 Introduction

The interest to the rapidly rotating systems has been recently rekindled thanks to the experimental observation of highly vortical quark-gluon plasma produced in the relativistic heavy-ion collisions [1–6]. Previous studies discussed the thermodynamics and the hydrodynamics of rotating systems based on the statistical approach [7–13], developed a quantum kinetic theory with spin degrees of freedom [14–22], and made predictions for the spin polarization measured in heavy-ion collisions [23–32], see for instance the reviews [33–35].

In [36, 37] we initiated a study of the electromagnetic radiation emitted by rapidly rotating systems. The advantage of the electromagnetic radiation is that it is only weakly affected by the plasma evolution. The idea is to observe the impact of rotation on the quantum fields.

The study in [36, 37] discussed "relatively slowly" rotating systems in magnetic field. Namely, we assumed that the magnetic length $1/\sqrt{eB}$ is much shorter than the inverse angular velocity Ω.[1] Such rotation is slow. On the other hand, the absolute value of the angular velocity satisfying this condition can be enormous, hence the qualifying adverb "relatively". Generally, we can say that a system is relatively slowly rotating if its transverse size a is much smaller than $1/\Omega$.

---

[1]We are using natural units where $c = \hbar = k_B = 1$.

Model simulations show that the vorticity of the quark-gluon plasma can be as high as its inverse transverse size a. This upsets the slow rotation assumption. A system rotating with the angular velocity Ω is causally connected only within the lightcone cylinder of radius $R = 1/\Omega$. When $R < a$ only a part of the rotating plasma is causally connected. This is a genuine fast rotation. Setting the proper boundary conditions on the quantum fields at the causal boundary becomes an essential procedure. In [38], in the spirit of the MIT bag model, we required that the radial current vanishes on the boundary. However, there may be other possible boundary conditions.

In the regime $1/\Omega < \ell$, where ℓ is the mean-free-path, the rotation is so fast that it overwhelms all inter-particle forces and pushes the matter towards the light-cylinder wall. Such a medium will break down to a set of rotating cylindrical regions of radii $R \ll a$. Within each cylindrical region the matter will be concentrated mostly at the boundary at R due to the centrifugal force. It seems reasonable therefore, that the dynamics of such extremely rapidly rotating system can be described by the quantum fields confined to the cylindrical surface of radius R. We will not be concerned with the statistical properties of the matter within the cylindrical region, since in view of $\ell > R$, it is simply an ideal rotating gas. Rather we are interested in the electromagnetic radiation it emits. Since the precise nature of the particles that make up the rotating cylinder is not very important — only the fact that they are found at the boundary is — we employ the scalar QED for calculations. It is reasonable to expect that the qualitative features of our results should be fairly model-independent.

The three rotation regimes of a system characterized by the radial size a, the light-cylinder radius $R = 1/\Omega$, the mean-free-path ℓ are

- *Slow rotation $\ell \ll a \ll R$.* This approximation is used in [36, 37].

- *Fast rotation $\ell \ll R \sim a$* [38, 39].

- *Extremely fast rotation $R \ll \ell \ll a$.* This is the scenario we consider in the paper.

In summary, we consider model in which the charged scalar particles can freely move on a thin cylindrical sheet of radius $R = 1/\Omega$ rotating with angular velocity Ω. In the following sections we will compute the electromagnetic radiation by a single particle and by a system of particles in thermal equilibrium. We believe that this model describes the universal properties of extremely rapidly rotating systems.
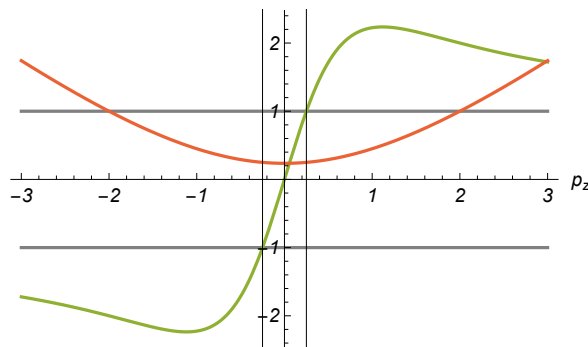
2 Radiation by scalar particle on cylindrical sheet

The wave function of a scalar particle of mass M embedded into a cylindrical surface rotating with the angular velocity Ω about its symmetry axis z is

$$\psi(t, \phi, z) = \frac{1}{\sqrt{2\pi L}} \frac{1}{\sqrt{2E}} e^{-iEt + ip_z z + im\phi} \,, \tag{2.1}$$

where energy spectrum is

$$E = \sqrt{p_z^2 + \frac{m^2}{R^2} + M^2} + m\Omega \,. \tag{2.2}$$

Figure 1. (Color online) $m\Omega = -2$, $M = 1$. Green line: $v(p_z)$, red line: $E(p_z)$. The allowed values: $-\frac{1}{4} \leq p_z \leq \frac{1}{4}$ corresponding to the box in the center.

The magnetic quantum number m is an integer, while the longitudinal momentum p_z is continuous assuming that the cylinder height L is very large. We note that $E > 0$ for any m.

The velocity of the quasi-classical motion along the z-direction is $v = p_z/E$. Clearly, only the states with $|v| \leq 1$ are causally connected. Inspection of (2.2) reveals that when $m \geq 0$, then $E > |p_z|$ for any value of p_z. In contrast, when $m < 0$ this condition is satisfied only when

$$|p_z| \leq \frac{M^2}{2|m|\Omega}, \quad \text{if} \quad m < 0. \tag{2.3}$$

Figure 1 shows an example of the dispersion relation (2.2) with $m < 0$. Vertical lines indicated the allowed range of p_z's.

We are interested to compute the electromagnetic radiation by this particle. The S_{fi}-matrix element reads

$$S_{fi} = -ie \int dt \int d\phi \int dz \, \boldsymbol{j}_{fi}(t,\phi,z) \cdot \boldsymbol{A}^*(t,\phi,z,R), \tag{2.4}$$

where the photon wave function in the Coulomb gauge is

$$\boldsymbol{A}(t,\phi,z,R) = \frac{1}{\sqrt{2\omega V}} \boldsymbol{\epsilon}_\lambda e^{i\boldsymbol{k}\cdot\boldsymbol{r}-i\omega t}, \quad \boldsymbol{\epsilon}_\lambda \cdot \boldsymbol{k} = 0, \tag{2.5}$$

and V is the system volume. The transition current is

$$\boldsymbol{j}_{fi} = i(\psi\boldsymbol{\nabla}\psi'^* - \psi'^*\boldsymbol{\nabla}\psi). \tag{2.6}$$

In our notation: $\psi_i = \psi$, $\psi_f = \psi'$.

Substituting (2.1) and (2.5) into (2.4) we arrive at

$$S_{fi} = \frac{-ie(2\pi)^2}{2\pi L\sqrt{2\omega V}2\sqrt{EE'}}\delta(E - E' - \omega)\delta(p_z - p_z' - k_z)$$
$$\times \boldsymbol{\epsilon}_\lambda^* \cdot \left[\frac{1}{R}\boldsymbol{e}_\phi(m + m') + \boldsymbol{e}_z(p_z + p_z')\right]2\pi i J_{m-m'}(k_\perp R). \tag{2.7}$$

Two convenient photon polarizations (following [40]):

$$\boldsymbol{\epsilon}_1 = -\boldsymbol{e}_\phi\,, \quad \boldsymbol{\epsilon}_2 = -\sin\theta\boldsymbol{e}_z + \cos\theta\boldsymbol{e}_\perp\,. \tag{2.8}$$

where θ is the polar angle defined with respect to the z-axis, e.g. $k_z = \omega\cos\theta$. The photon transverse momentum is then $k_\perp = \omega\sin\theta$.

The photon emission rate can be computed as

$$\dot{w}_{fi} = \sum_\lambda \sum_{m'} \frac{|S_{fi}|^2}{T} \frac{dk_z L}{2\pi} \frac{dk_\perp k_\perp \pi R^2}{2\pi} \frac{dp_z L}{2\pi} \tag{2.9}$$

while the radiation intensity is given by $W = \dot{w}_{fi}\omega$:

$$W = \sum_{m'=-\infty}^{m-1} \frac{e^2}{16\pi E E'} \delta(E - E' - \omega) \left[\frac{(m+m')^2}{R^2} + \sin^2\theta(p_z + p_z')^2 \right] J_{m-m'}^2(k_\perp R) dk_z dk_\perp k_\perp\,. \tag{2.10}$$

The sum over the negative m' in (2.10) is constrained by (2.3). One can expresses $dk_z dk_\perp k_\perp = \omega^2 d\omega d\sin\theta = \omega^2 d\omega do/2\pi$, where do is the element of the solid angle in the direction of the emitted photon. In the non-relativistic limit, the leading term in the multipole expansion of the intensity is the magnetic dipole one because the electric dipole moment vanishes while the magnetic moment $\boldsymbol{\mu} = \frac{1}{2}e\boldsymbol{r}\times\boldsymbol{v}$ is finite.

The delta-function in (2.10) can be re-written as

$$\delta(E - E' - \omega) = \frac{\delta(\omega - \omega_0)(E' - m'\Omega)}{E - m'\Omega - \omega\sin^2\theta - p_z\cos\theta}\,. \tag{2.11}$$

where the characteristic frequency is

$$\omega_0 = \frac{1}{\sin^2\theta}\Bigg\{ E - m'\Omega - p_z\cos\theta \tag{2.12}$$

$$- \sqrt{(E - m'\Omega - p_z\cos\theta)^2 - \sin^2\theta\left[(E - m'\Omega)^2 - p_z^2 - m'^2/R^2 - M^2\right]}\Bigg\}\,.$$

Taking the integral over ω one is left with the angular spectrum dW/do. Alternatively, we can cast the delta-function in the form

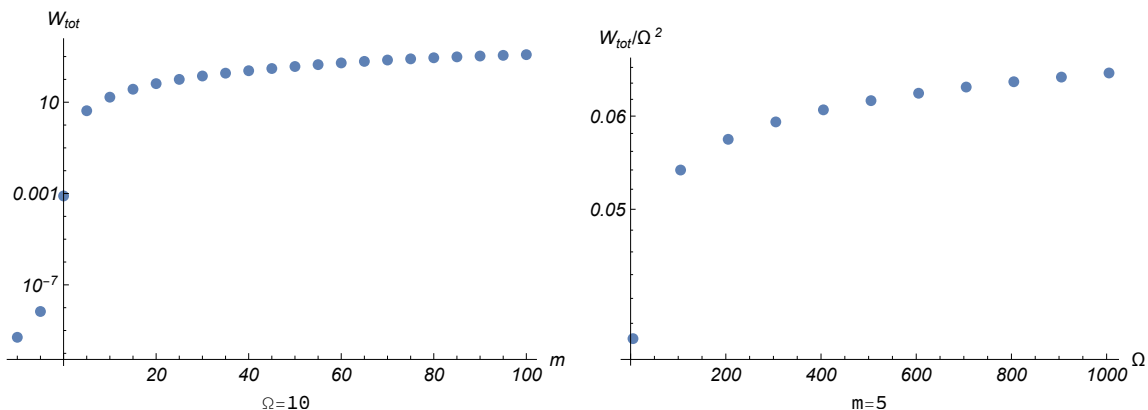$$\delta(E - E' - \omega) = \sum_\pm \frac{\delta(\cos\theta - \cos\theta_\pm)(E' - m'\Omega)}{\omega|\omega\cos\theta - p_z|}\,, \tag{2.13}$$

where

$$\cos\theta_\pm = \frac{1}{\omega}\left\{ p_z \pm \sqrt{(E - m'\Omega - \omega)^2 - m'^2/R^2 - M^2} \right\}\,. \tag{2.14}$$

We note that in order that $|\cos\theta_\pm| \leq 1$, photon energy ω must not be too small. For the states with $m' < 0$ one has to take into account the requirement (2.3).

The radiation intensity is shown in figure 2 as a function of m and Ω.

Figure 2. Left panel: W vs m at $p_z = 0$, right panel: W/Ω^2 vs Ω. In both panels $M = 1$.

3 Radiation intensity by a single particle at rest

To investigate the radiation intensity analytically, consider a reference frame in which the incident particle is at rest in the axial direction: $p_z = 0$, $p'_z = -\omega \cos\theta$. In particular, (2.3) becomes

$$\omega_0 |\cos\theta| \leq \frac{M^2}{2|m'|\Omega} \, . \tag{3.1}$$

In addition, we will focus on the limit $\Omega \gg M$. In this case the spectrum (2.2) reads

$$E \approx \begin{cases} 2m\Omega \, , & m > 0 \, ; \\ M \, , & m = 0 \, ; \\ \frac{M^2}{2|m|\Omega} \, , & m < 0 \, . \end{cases} \qquad E' \approx \begin{cases} \sqrt{p'^2_z + m'^2\Omega^2} + m'\Omega \, , & m' > 0 \, ; \\ \sqrt{p'^2_z + M^2} \, , & m' = 0 \, ; \\ \frac{p'^2_z + M^2}{2|m'|\Omega} \, , & m' < 0 \, . \end{cases} \tag{3.2}$$

In order that $E > E'$, the range of m' must be $m' \leq m - 1$.

We distinguish three cases: (A) $m > 0$, (B) $m = 0$ and (C) $m < 0$.

3.1 $m > 0$

Figure 3 shows the dependence of a single term in the sum (2.10) on m' for $m > 0$. The mode with $m' = 0$ is enhanced over those with $m' > 0$ which in turn are enhanced as compared to the modes $m' < 0$. To understand the dynamics in each case and find an appropriate approximation we split the summation over m' into three parts: (A1) $m' \leq -1$, (A2) $m' \geq 1$ and (A3) $m' = 0$.
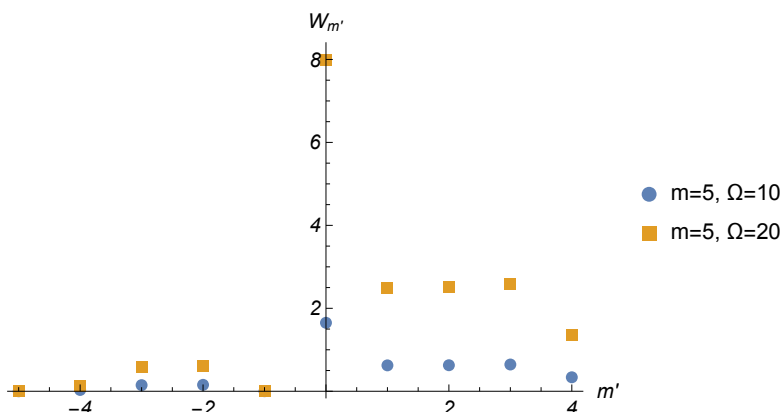
Figure 3. (Color online) The radiation intensity $W_{m'}$ of a single term in (2.10) for $m = 5$ vs m'. The total intensity W is the sum of all $W_{m'}$. The blue and orange symbols overlap at $m' = -1$.

3.1.1 $m' < 0$

Using (3.2), (2.11), (2.12) in (2.10) and keeping the leading terms in M/Ω we obtain

$$
\begin{aligned}
W^{A1} &= \frac{e^2}{2\pi} \sum_{m'=-\infty}^{-1} \int_0^\pi \frac{1}{16\pi EE'} \frac{\delta(2m\Omega - \omega)}{\frac{\omega \cos^2\theta}{E' - m'\Omega} + 1} \left[\frac{(m+m')^2}{R^2} + \sin^2\theta\cos^2\theta\,\omega^2 \right] \\
&\quad \times J_{m-m'}^2(k_\perp R)\omega^2 \eta\left(M^2 + 2m'\Omega\omega|\cos\theta|\right) d\omega \sin\theta\, d\theta \quad\quad (3.3) \\
&= \frac{e^2}{2\pi} \sum_{m'=-\infty}^{-1} 2 \int_0^1 \frac{E' - m'\Omega}{16\pi EE'(2m\Omega\cos^2\theta + E' - m'\Omega)} \left[\frac{(m+m')^2}{R^2} + (1-x^2)x^2(2m\Omega)^2 \right] \\
&\quad \times J_{m-m'}^2\left(2m\sqrt{1-x^2}\right)(2m\Omega)^2 \eta\left(M^2 + 2m'\Omega\omega x\right) dx,\quad\quad (3.4)
\end{aligned}
$$

where η is the step function accounting for (3.1), $x = \cos\theta$ and we took advantage of the fact that the integrals over $0 \le x \le 1$ and $-1 \le x \le 0$ are equal. In view of (3.2) and (3.1), the angular integration is confined to the small region

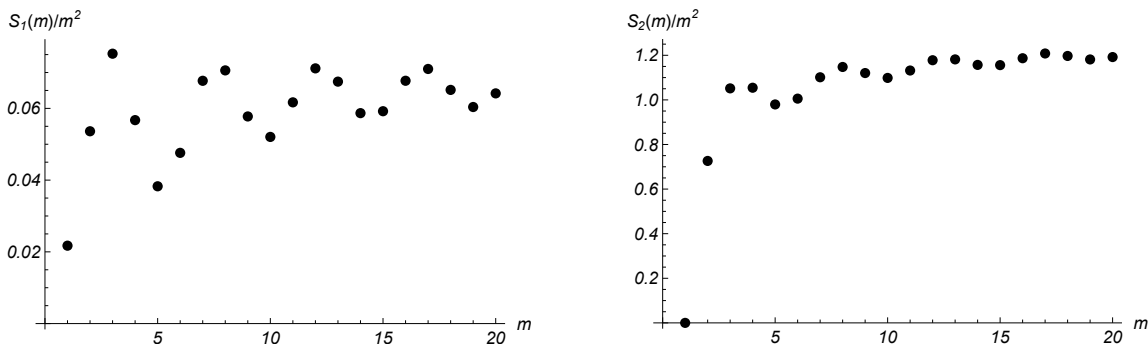$$
x < \frac{M^2}{4\Omega^2 m|m'|} \ll 1. \quad\quad (3.5)
$$

Bearing this in mind and using (3.2) we can then write $\omega_0 \cos^2\theta + E' \approx \frac{M^2}{2|m'|\Omega} \ll \Omega$. After expanding the remaining terms in x we obtain

$$
W^{A1} = \frac{e^2\Omega^2}{8\pi} \sum_{j=1}^\infty (m-j)^2 J_{m+j}^2(2m) = \frac{e^2\Omega^2}{8\pi} S_1(m), \qu\quad (3.6)
$$

where $j = -m'$ and we defined

$$
S_1(m) = \sum_{j=1}^\infty (m-j)^2 J_{m+j}^2(2m). \qu\quad (3.7)
$$

This function is shown in figure 4.

Figure 4. Left panel: $S_1(m)/m^2$, right panel: $S_2(m)/m^2$ appearing in (3.7) and (3.10) respectively.

3.1.2 $m' > 0$

Now consider the final states with $m' > 0$. In this case the constraint (3.1) does not apply. It implies that we can safely neglect M in (2.12), assuming that the integral over θ is finite at $\theta = \pi/2$ (which is indeed the case as will be seen shortly). Thus,

$$\omega_0 \approx \frac{\Omega}{\sin^2\theta}\left\{2m - m' - \sqrt{(2m-m')^2 - 4m(m-m')\sin^2\theta}\right\} \equiv \Omega z\,, \qquad (3.8)$$

and $E' = 2\Omega m - \omega_0$. A simple calculation yields

$$W^{A2} = \frac{e^2\Omega^2}{32\pi}S_2\left(m\right)\,, \qquad (3.9)$$

where we defined the function

$$S_2(m) = \sum_{m'=1}^{m-1}\int_0^\pi \frac{(2m-m'-z)\left[(m+m')^2 + z^2\sin^2\theta\cos^2\theta\right]}{m(2m-z)(2m-m'-z\sin^2\theta)}J^2_{m-m'}(z\sin\theta)z^2\sin\theta d\theta \qquad (3.10)$$

which depends only on m. The numerical calculation of S_2 is shown in figure 4.

3.1.3 $m' = 0$

In this case the photon frequencies are

$$\omega_0 = \frac{2m\Omega}{\sin^2\theta}\left\{1 - \sqrt{\cos^2\theta + \sin^2\theta\frac{M^2}{4m^2\Omega^2}}\right\} \qquad (3.11)$$

and the intensity is

$$W^{A3} = \frac{e^2}{16\pi(2m\Omega)}\int_0^\pi \frac{m^2\Omega^2 + \omega_0^2\sin^2\theta\cos^2\theta}{\omega_0\cos^2\theta + \sqrt{\omega_0^2\cos^2\theta + M^2}}J^2_m(\omega_0 R\sin\theta)\omega_0^2\sin\theta d\theta\,. \qquad (3.12)$$

The integrand peaks at small $x = \cos\theta$ which gives rise to the logarithmically enhanced contribution. In this leading logarithmic approximation we write

$$W^{A3} \approx \frac{e^2}{16\pi}2\int_0^1 \frac{m^2\Omega^2}{x^2 + \sqrt{x^2 + \frac{M^2}{4m^2\Omega^2}}}J^2_m(2m)dx \approx \frac{e^2\Omega^2}{8\pi}m^2 J^2_m(2m)\log\frac{4m\Omega}{M}\,. \qquad (3.13)$$

3.2 $m = 0$

In this case all finial states have $m' < 0$. Using (2.10)–(2.14) and replacing $-m' = j$ we get

$$W^B = \sum_{j=1}^{\infty} \frac{e^2(E' - m'\Omega)}{16\pi EE'(E' - m'\Omega + \omega_0 \cos^2\theta)} \left[\frac{j^2}{R^2} + \omega_0^2 \sin^2\theta \cos^2\theta\right] \eta\left(M^2 - 2j\Omega\omega|\cos\theta|\right)$$
$$\times J_j^2(\omega_0 R \sin\theta)\omega_0^2 \sin\theta d\theta\,, \tag{3.14}$$

where, considering that $x = \cos\theta \ll 1$ (see (3.5)) we approximate:

$$\omega_0 \approx M\left(1 - \frac{M}{2j\Omega}(1 + x^2)\right)\,. \tag{3.15}$$

It follows that $E' + \omega_0 \cos^2\theta + j\Omega \approx j\Omega$. We are now left with a trivial integral over x which yields:

$$W^B = \frac{e^2\Omega^2}{8\pi} \sum_{j=1}^{\infty} j^2 J_j^2(MR) \tag{3.16}$$

Expanding the Bessel function and keeping only the leading term with $j = 1$ we finally obtain

$$W^B = \frac{e^2 M^2}{32\pi}\,. \tag{3.17}$$

3.3 $m < 0$

This is the most unusual case because the fermion transitions occur between the levels with negative m and m' which correspond to $0 < E' < E < M$. First deal with the delta-function:

$$\delta\left(-\frac{M^2}{2m\Omega} + \frac{\omega^2\cos^2\theta + M^2}{2m'\Omega} - \omega\right) = \frac{1}{\frac{\omega\cos^2\theta}{m'\Omega} - 1}\delta\left(\omega - \frac{M^2(|m'| - |m|)}{2|m'||m|\Omega}\right)\,. \tag{3.18}$$

were we used (3.2). We get for the intensity using (2.10):

$$W^C = \frac{e^2}{16\pi} \sum_{m'=-\infty}^{m-1} \frac{2|m|\Omega}{M^2} \frac{2|m'|\Omega}{\omega_0^2 \cos^2\theta + M^2} \frac{|m'|\Omega}{\omega_0 \cos^2\theta + |m'|\Omega} \left[\frac{(m + m')^2}{R^2} + \omega_0^2 \sin^2\theta \cos^2\theta\right]$$
$$\times \eta\left(M^2 + 2m'\Omega\omega|\cos\theta|\right) J_{m-m'}^2(\omega_0 R \sin\theta)\omega_0^2 \sin\theta d\theta\,. \tag{3.19}$$

In view of (3.18), the step function implies that $|\cos\theta| \leq |m|/\nu$, where $\nu = |m'| - |m|$ is a positive integer. Since $\omega_0 \sim M^2/\Omega$, we can neglect it in the denominators and in the square brackets in (3.19). It also allows us to expand the Bessel function $J_\nu(\xi) \approx \frac{1}{\nu!}(\xi/2)^\nu$ and retain only the leading $\nu = 1$ term. Since $|m| > 1$ in this section, $\cos\theta$ is not restricted at all in this approximation. The angular integration becomes trivial and yields

$$W^C = \frac{e^2 M^4}{192\pi\Omega^2} \frac{(2|m| + 1)^2}{|m|^3(|m| + 1)^3}\,. \tag{3.20}$$

3.4 Summary of $\Omega \gg M$ approximation

In summary, the radiation intensity at $\Omega \gg M$ is given by

$$W = \frac{e^2\Omega^2}{8\pi} \begin{cases} S_1(m) + \frac{1}{4}S_2(m) + m^2 J_m^2(2m)\log\frac{4m\Omega}{M} \,, & m > 0 \,, \\ \frac{M^2}{4\Omega^2} \,, & m = 0 \,, \\ \frac{M^4}{24\Omega^4}\frac{(2|m|+1)^2}{|m|^3(|m|+1)^3} \,, & m < 0 \,. \end{cases} \tag{3.21}$$

The transitions from $m > 0$, with the corresponding energy $E \approx 2\Omega m$, give the largest contribution. When m is not very large, the leading channel is the transition to $m' = 0$ ($E' \approx M \ll E$) given by (3.13). This is also seen in figure 3. For large m, we can use the well-known formula (see e.g. **9.3.15** in [41])

$$J_m(2m) \approx \sqrt{\frac{2}{\pi\sqrt{3}m}}\cos\left[m(\sqrt{3}-\pi/3)-\pi/4\right], \quad m \gg 1 \,, \tag{3.22}$$

to conclude that the contribution from the transitions to $m' > 0$ becomes dominant since $S_2(m) \sim m^2$. We verified that (3.21) is an accurate approximation of the exact formula at $p_z = 0$ and $M \ll \Omega$ (plotted in figure 2).

4 Radiation by spinning ideal gas

4.1 Energy spectrum

If an ideal Maxwell-Boltzmann gas rotates extremely rapidly, then its radiation intensity is given by

$$I = \sum_{m=-\infty}^{\infty} \int \frac{dp_z L}{2\pi} \int do \int_0^E d\omega \frac{dW}{do\,d\omega} e^{-\beta E} \,. \tag{4.1}$$

Using (2.10), (2.13) and (2.14) we obtain

$$\frac{dI}{Ld\omega} = \frac{e^2}{16\pi}\sum_{m=-\infty}^{\infty}\sum_{\pm}\sum_{m'=-\infty}^{m-1}\int\frac{dp_z}{2\pi}e^{-\beta E}\frac{E' - m'\Omega}{EE'\omega|\omega\cos\theta_\pm - pz|}$$
$$\times \left[\frac{(m+m')^2}{R^2} + \sin^2\theta_\pm(2p_z - \omega\cos\theta_\pm)^2\right]J_{m-m'}^2(\omega R\sin\theta_\pm)\omega^2 \,. \tag{4.2}$$

where the integral over p_z is restricted by (2.3) for $m < 0$. The corresponding energy spectra are exhibited in figure 5. We observe that there is the threshold frequency below which photon emission is impossible. We also notice that the spectrum peaks at $\omega \sim \Omega$.

4.2 Photon production in heavy-ion collisions

It is tempting to apply the model developed in this article to describe the photon production by rotating quark-gluon plasma. We certainly realize that the plasma is not yet in the regime of extremely fast rotation $\Omega > \ell^{-1}$. On the other hand, it is already in the region of fast rotation $\Omega \sim a^{-1}$, using the notation introduced in Introduction. We therefore
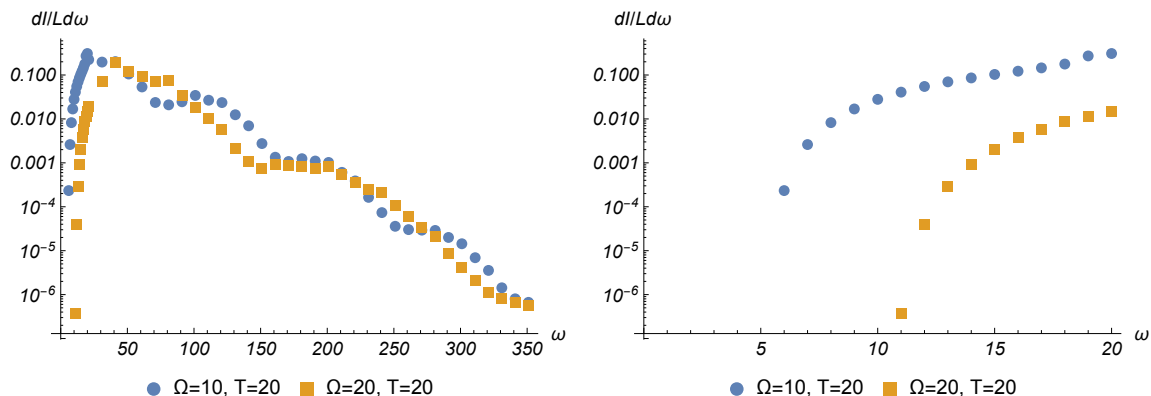
Figure 5. (Color online) The energy spectrum of electromagnetic radiation by a thermal system. Right panel zooms into the infrared region of the left one. $M = 1$.

consider the calculation of the photon spectrum as the no more than a back-of-the-envelop estimate and the proof of principle that rotation is a relevant effect.

The photon emission from quark-gluon plasma, is described in terms of the following variables: k_T, the photon momentum in the plane perpendicular to the collision axis (not to be confused with $k_\perp$ defined with respect to the rotation axis), ϕ its azimuthal angle in that plane and y its rapidity. They are related to the photon energy ω and the emission angle θ (see [42] for more details):

$$\omega = k_T \cosh y, \quad \cos\theta = \sin\phi/\cosh y. \tag{4.3}$$

We now express the photon spectrum as

$$\frac{dN(k_T, y, \phi)}{k_T dk_T d\phi dy} = g\Delta t \frac{dI(\omega, \theta)}{\omega^2 d\omega do}, \tag{4.4}$$

where Δt is the time interval. In realistic case photons are emitted by fermions with two possible polarizations and three colors and three flavors which make up the degeneracy factor $g = 18$. Eq. (4.4) simplifies at the midrapidity region $y = 0$:

$$\frac{dN}{k_T dk_T dy}\bigg|_{y=0} = \frac{g\Delta t L}{k_T^2} \int_0^{2\pi} d\phi \frac{dI}{Ld\omega do}\bigg|_{\omega=k_T, \theta=\frac{\pi}{2}-\phi}. \tag{4.5}$$

The intensity I is given by (4.1) and W is given by (2.10).

It is now advantageous to use the delta-function in (2.10) to take the integral over p_z. To this end we write

$$\delta(E - E' - \omega) = \delta\left(\sqrt{p_z^2 + m^2\Omega^2 + M^2} - \sqrt{(p_z - \omega\cos\theta)^2 + m'^2\Omega^2 + M^2} + \Delta\right)$$
$$= \frac{\delta(p_z - p_{z0})(E - m\Omega)(E - \omega - m'\Omega)}{|\omega\cos\theta(E - m\Omega) + p_z\Delta|}, \tag{4.6}$$

where we introduced a convenient notation

$$\Delta = (m - m')\Omega - \omega. \tag{4.7}$$

To compute p_{z0} we rewrite the equation in the second delta-function in (4.6) as a quadratic equation for p_z. Of course not all its solutions necessarily satisfy the original equation. A careful examination of its two roots reveals that one root satisfies it at $\Delta > 0$, while another one at $\Delta < 0$. These can be combined in a single formula:

$$p_{z0} = \frac{1}{2(\Delta^2 - \omega^2 \cos^2 \theta)} \Big\{ -\omega \cos \theta(\omega^2 \cos^2 \theta - \Delta^2 + m^2\Omega^2 - m'^2\Omega^2) \tag{4.8}$$
$$+ \Delta\sqrt{(\omega^2 \cos^2 \theta - \Delta^2 + m^2\Omega^2 - m'^2\Omega^2)^2 + 4(m^2\Omega^2 + M^2)(\omega^2 \cos^2 \theta - \Delta^2)} \Big\},$$

provided that

$$\Delta^2 - \omega^2 \cos^2 \theta \leq 0. \tag{4.9}$$

Using (4.7) in (4.9) and noting that $|\cos \theta| \leq 1$ we find that the allowed photon energies are

$$\omega \geq \frac{1}{2}(m - m')\Omega. \tag{4.10}$$

In particular, the photon spectrum has an infrared threshold at $\omega_{\min} = \Omega/2$. This is indeed clearly seen in figure 5. Eq. (4.9) is a constraint on the allowed values of the photon emission angle:

$$|\theta| \leq \Theta = \arcsin \sqrt{1 - \Delta^2/\omega^2}. \tag{4.11}$$

Taking all these into account we obtain the final expression for the photon spectrum:

$$\frac{dN}{k_T dk_T dy}\Big|_{y=0} = \frac{g\Delta t L e^2}{4(2\pi)^3} \sum_{m=-\infty}^{\infty} \sum_{m'=-\infty}^{m-1} \int_{-\Theta}^{+\Theta} d\theta \frac{1}{EE'} e^{-E/T} \frac{(E - m\Omega)(E' - m'\Omega)}{|k_T \cos \theta(E - m\Omega) + p_z\Delta|}$$
$$\times \left[(m + m')^2\Omega^2 + \sin^2 \theta(2p_{z0} - k_T \cos \theta)^2 \right] J_{m-m'}^2(k_T \sin \theta \Omega^{-1}), \quad (4.12)$$

valid for $k_T = \omega$ satisfying (4.10). E and E' are the functions of p_{z0}. At negative m and m' the angular integration is further restricted by (2.3). However, as we have seen, the negative m and m' give a negligible contribution. Therefore in practice the sums over m and m' rum only over the non-negative values.

The results of the calculation are shown in figure 6 along with the experimental data on photon production in relativistic heavy-ion collisions [43]. We observe a wondrous agreement for a particular plasma temperature. This does not of course imply that plasma rotation is the only source of photons. However, it does indicate that it must be accounted for in comprehensive phenomenological models. And perhaps it will help resolving the long-standing puzzle of the photon excess at low momenta.

5 Summary

We posited that systems rotating with extreme angular velocity $\Omega \sim \ell^{-1}$, where ℓ is the mean-free-path, can be described by matter fields confined to the two dimensional
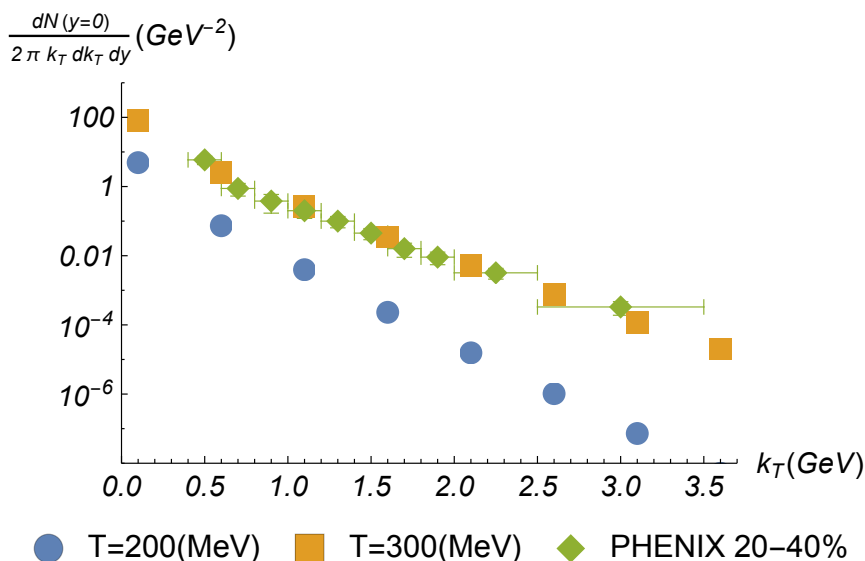
Figure 6. (Color online) Photon spectrum at two temperatures and $\Omega = 0.1\,\mathrm{fm}^{-1}$. The data is from [43]. $\Delta t = 10\,\mathrm{fm}/c$, $L = 10\,\mathrm{fm}$, $M = 150\,\mathrm{MeV}$.

cylindrical surface of radius $R = 1/\Omega$. We developed an application of this idea to the photon production by the rotating quark-gluon plasma and argued that it is consistent with the experimental observations.

The statistical properties inside the light-cylinder are equivalent to those of the two-dimensional ideal gas, as the interactions are screened by $R < \ell$. However, the statistical properties of the entire plasma are determined by the interaction of the light-cylinders; the development of these ideas is left for another study.

Acknowledgments

Open Access. This article is distributed under the terms of the Creative Commons Attribution License ([CC-BY 4.0](#)), which permits any use, distribution and reproduction in any medium, provided the original author(s) and source are credited.

References

[1] STAR collaboration, *Global Λ hyperon polarization in nuclear collisions: evidence for the most vortical fluid*, *Nature* **548** (2017) 62 [arXiv:1701.06657] [INSPIRE].

[2] STAR collaboration, *Global polarization of Λ hyperons in Au+Au collisions at $\sqrt{s_{\mathrm{NN}}} = 200\,GeV$*, *Phys. Rev. C* **98** (2018) 014910 [arXiv:1805.04400] [INSPIRE].

[3] STAR collaboration, *Polarization of $\Lambda(\bar{\Lambda})$ hyperons along the beam direction in Au+Au collisions at $\sqrt{s_{\mathrm{NN}}} = 200\,GeV$*, *Phys. Rev. Lett.* **123** (2019) 132301 [arXiv:1905.11917] [INSPIRE].

[4] ALICE collaboration, *Evidence of spin-orbital angular momentum interactions in relativistic heavy-ion collisions*, *Phys. Rev. Lett.* **125** (2020) 012301 [`arXiv:1910.14408`] [ɪɴSPIRE].

[5] STAR collaboration, *Global polarization of Ξ and Ω hyperons in Au+Au collisions at $\sqrt{s_{NN}} = 200\, GeV$*, *Phys. Rev. Lett.* **126** (2021) 162301 [*Erratum ibid.* **131** (2023) 089901] [`arXiv:2012.13601`] [ɪɴSPIRE].

[6] STAR collaboration, *Global Λ-hyperon polarization in Au+Au collisions at $\sqrt{s_{NN}} = 3\, GeV$*, *Phys. Rev. C* **104** (2021) L061901 [`arXiv:2108.00044`] [ɪɴSPIRE].

[7] D.N. Zubarev, A.V. Prozorkevich and S.A. Smolyanskii, *Derivation of nonlinear generalized equations of quantum relativistic hydrodynamics*, *Theor. Math. Phys.* **40** (1979) 821 [ɪɴSPIRE].

[8] A. Vilenkin, *Quantum field theory at finite temperature in a rotating system*, *Phys. Rev. D* **21** (1980) 2260 [ɪɴSPIRE].

[9] T. Hayata, Y. Hidaka, T. Noumi and M. Hongo, *Relativistic hydrodynamics from quantum field theory on the basis of the generalized Gibbs ensemble method*, *Phys. Rev. D* **92** (2015) 065008 [`arXiv:1503.04535`] [ɪɴSPIRE].

[10] V.E. Ambrus and E. Winstanley, *Rotating fermions inside a cylindrical boundary*, *Phys. Rev. D* **93** (2016) 104014 [`arXiv:1512.05239`] [ɪɴSPIRE].

[11] M. Buzzegoli, E. Grossi and F. Becattini, *General equilibrium second-order hydrodynamic coefficients for free quantum fields*, *JHEP* **10** (2017) 091 [*Erratum ibid.* **07** (2018) 119] [`arXiv:1704.02808`] [ɪɴSPIRE].

[12] F. Becattini, M. Buzzegoli and E. Grossi, *Reworking the Zubarev's approach to non-equilibrium quantum statistical mechanics*, *Particles* **2** (2019) 197 [`arXiv:1902.01089`] [ɪɴSPIRE].

[13] D. Montenegro and G. Torrieri, *Linear response theory and effective action of relativistic hydrodynamics with spin*, *Phys. Rev. D* **102** (2020) 036007 [`arXiv:2004.10195`] [ɪɴSPIRE].

[14] N. Weickgenannt et al., *Kinetic theory for massive spin-1/2 particles from the Wigner-function formalism*, *Phys. Rev. D* **100** (2019) 056018 [`arXiv:1902.06513`] [ɪɴSPIRE].

[15] J.-H. Gao and Z.-T. Liang, *Relativistic quantum kinetic theory for massive fermions and spin effects*, *Phys. Rev. D* **100** (2019) 056021 [`arXiv:1902.06510`] [ɪɴSPIRE].

[16] K. Hattori, Y. Hidaka and D.-L. Yang, *Axial kinetic theory and spin transport for fermions with arbitrary mass*, *Phys. Rev. D* **100** (2019) 096011 [`arXiv:1903.01653`] [ɪɴSPIRE].

[17] S. Bhadury et al., *Dissipative spin dynamics in relativistic matter*, *Phys. Rev. D* **103** (2021) 014030 [`arXiv:2008.10976`] [ɪɴSPIRE].

[18] Y.-C. Liu, K. Mameda and X.-G. Huang, *Covariant spin kinetic theory I: collisionless limit*, *Chin. Phys. C* **44** (2020) 094101 [*Erratum ibid.* **45** (2021) 089001] [`arXiv:2002.03753`] [ɪɴSPIRE].

[19] N. Weickgenannt et al., *Generating spin polarization from vorticity through nonlocal collisions*, *Phys. Rev. Lett.* **127** (2021) 052301 [`arXiv:2005.01506`] [ɪɴSPIRE].

[20] S. Shi, C. Gale and S. Jeon, *From chiral kinetic theory to relativistic viscous spin hydrodynamics*, *Phys. Rev. C* **103** (2021) 044906 [`arXiv:2008.08618`] [ɪɴSPIRE].

[21] N. Weickgenannt, D. Wagner, E. Speranza and D.H. Rischke, *Relativistic second-order dissipative spin hydrodynamics from the method of moments*, *Phys. Rev. D* **106** (2022) 096014 [arXiv:2203.04766] [INSPIRE].

[22] Y. Hidaka, S. Pu and D.-L. Yang, *Nonlinear responses of chiral fluids from kinetic theory*, *Phys. Rev. D* **97** (2018) 016004 [arXiv:1710.00278] [INSPIRE].

[23] I. Karpenko and F. Becattini, *Study of Λ polarization in relativistic nuclear collisions at $\sqrt{s_{\mathrm{NN}}} = 7.7$–200 GeV*, *Eur. Phys. J. C* **77** (2017) 213 [arXiv:1610.04717] [INSPIRE].

[24] Y. Xie, D. Wang and L.P. Csernai, *Global Λ polarization in high energy collisions*, *Phys. Rev. C* **95** (2017) 031901 [arXiv:1703.03770] [INSPIRE].

[25] H.-Z. Wu, L.-G. Pang, X.-G. Huang and Q. Wang, *Local spin polarization in high energy heavy ion collisions*, *Phys. Rev. Research.* **1** (2019) 033058 [arXiv:1906.09385] [INSPIRE].

[26] Y.B. Ivanov, *Global Λ polarization in moderately relativistic nuclear collisions*, *Phys. Rev. C* **103** (2021) L031903 [arXiv:2012.07597] [INSPIRE].

[27] B. Fu, K. Xu, X.-G. Huang and H. Song, *Hydrodynamic study of hyperon spin polarization in relativistic heavy ion collisions*, *Phys. Rev. C* **103** (2021) 024903 [arXiv:2011.03740] [INSPIRE].

[28] H. Li, L.-G. Pang, Q. Wang and X.-L. Xia, *Global Λ polarization in heavy-ion collisions from a transport model*, *Phys. Rev. C* **96** (2017) 054908 [arXiv:1704.01507] [INSPIRE].

[29] D.-X. Wei, W.-T. Deng and X.-G. Huang, *Thermal vorticity and spin polarization in heavy-ion collisions*, *Phys. Rev. C* **99** (2019) 014905 [arXiv:1810.00151] [INSPIRE].

[30] Y.B. Ivanov, V.D. Toneev and A.A. Soldatov, *Estimates of hyperon polarization in heavy-ion collisions at collision energies $\sqrt{s_{\mathrm{NN}}} = 4$–40 GeV*, *Phys. Rev. C* **100** (2019) 014908 [arXiv:1903.05455] [INSPIRE].

[31] Y. Guo et al., *Hyperon polarization from the vortical fluid in low-energy nuclear collisions*, *Phys. Rev. C* **104** (2021) L041902 [arXiv:2105.13481] [INSPIRE].

[32] S. Alzhrani, S. Ryu and C. Shen, *Λ spin polarization in event-by-event relativistic heavy-ion collisions*, *Phys. Rev. C* **106** (2022) 014905 [arXiv:2203.15718] [INSPIRE].

[33] W. Florkowski, A. Kumar and R. Ryblewski, *Relativistic hydrodynamics for spin-polarized fluids*, *Prog. Part. Nucl. Phys.* **108** (2019) 103709 [arXiv:1811.04409] [INSPIRE].

[34] F. Becattini, J. Liao and M. Lisa eds., *Strongly interacting matter under rotation*, *Lect. Notes Phys.* **987** (2021) 1.

[35] F. Becattini and M.A. Lisa, *Polarization and vorticity in the quark-gluon plasma*, *Ann. Rev. Nucl. Part. Sci.* **70** (2020) 395 [arXiv:2003.03640] [INSPIRE].

[36] M. Buzzegoli, J.D. Kroth, K. Tuchin and N. Vijayakumar, *Synchrotron radiation by slowly rotating fermions*, *Phys. Rev. D* **107** (2023) L051901 [arXiv:2209.02597] [INSPIRE].

[37] M. Buzzegoli, J.D. Kroth, K. Tuchin and N. Vijayakumar, *Photon radiation by relatively slowly rotating fermions in magnetic field*, *Phys. Rev. D* **108** (2023) 096014 [arXiv:2306.03863] [INSPIRE].

[38] M. Buzzegoli and K. Tuchin, *Chiral magnetic effect in a cylindrical domain*, *Phys. Rev. D* **108** (2023) 056008 [arXiv:2305.13149] [INSPIRE].

[39] M. Buzzegoli and K. Tuchin, *Bound states and electromagnetic radiation of relativistically rotating cylindrical wells*, *Nucl. Phys. A* **1030** (2023) 122577 [arXiv:2209.03991] [INSPIRE].

[40] A.A. Sokolov, I.M. Ternov and C.W. Kilmister, *Radiation from relativistic electrons*, American Institute of Physics, U.S.A. (1986).

[41] M. Abramowitz and I.A. Stegun, *Handbook of mathematical functions with formulas, graphs, and mathematical tables*, U.S. Government printing office, U.S.A. (1968).

[42] K. Tuchin, *Role of magnetic field in photon excess in heavy ion collisions*, *Phys. Rev. C* **91** (2015) 014902 [arXiv:1406.5097] [INSPIRE].

[43] PHENIX collaboration, *Centrality dependence of low-momentum direct-photon production in Au+Au collisions at $\sqrt{s_{\mathrm{NN}}} = 200\,GeV$*, *Phys. Rev. C* **91** (2015) 064904 [arXiv:1405.3940] [INSPIRE].